Mass-Dependent and -Independent Fractionation of Hg Isotopes by Photoreduction in Aquatic Systems

Bridget A. Bergquist and Joel D. Blum

Mercury (Hg) isotopes can be used as tracers of Hg biogeochemical pathways in the environment. The photochemical reduction of aqueous Hg species by natural sunlight leads to both mass-dependent fractionation (MDF) of Hg isotopes and mass-independent fractionation (MIF) of the odd-mass isotopes, with the relation between the MIF for the two odd isotopes being distinct for different photoreduction pathways. Large variations in MDF and MIF are observed in fish and provide new insights into the sources and bioaccumulation of Hg in food webs. MIF in fish can also be used to estimate the loss of methylmercury via photoreduction in aquatic ecosytems.

Mercury (Hg) is a globally distributed and extremely toxic pollutant (*1*, *2*), and its mobility and bioaccumulation are highly dependent on speciation and reductive-oxidative cycling in the environment (*3*). Both inorganic and methylated Hg species have severe health effects in humans, but it is monomethylmercury (MeHg) that is thought to be the main species involved in bioaccumulation in the food web and human exposure via fish consumption (*4*). Human activities, such as coal combustion, and natural Hg fluxes release large amounts of inorganic Hg to the atmosphere either as a gas (Hg^0) or as the reactive Hg^{+2} species (*2*, *3*). In aquatic systems and sediments, a small fraction of the Hg^{+2} is transformed to the bioavailable MeHg form (*5*). Although Hg poses a proven health risk, much of the natural cycle of Hg is not well understood (*3*), and new approaches are necessary to better elucidate, track, and quantify Hg sources and transformations in the environment.

Stable isotope fractionation of light elements (C, H, O, S, and N) is widely used to identify and trace biogeochemical pathways. Recent analytical advancements, especially in multicollector inductively coupled plasma mass spectrometry (MC-ICPMS), have allowed for stable isotopic studies of many heavier elements [>40 atomic mass units (amu)], including Hg. Hg has seven stable isotopes (196, 198, 199, 200, 201, 202, and 204 amu) with a mass difference of 4%, active redox chemistry, a volatile form (Hg^0), and a tendency to form covalent bonds, thus providing many opportunities for isotopic fractionation. A large range in δ^{202}Hg values is observed in natural samples, with most samples displaying mass-dependent fractionation (MDF) (*6*–*12*). A small body of data also suggests that natural samples sometimes display mass-independent fractionation (MIF) of Hg isotopes (*13*, *14*). Only a few other isotopic systems have been shown to display MIF, the most notable of which are O and S (*15*–*17*). In both cases, the application of MIF has proven very useful in a number of fields, including cosmochemistry, paleoclimatology, physical chemistry, atmospheric chemistry, and biogeochemistry.

We documented MIF of Hg isotopes during a natural process, constrained the potential mechanism of isotope fractionation, and applied the MIF observed in natural samples to quantify the photochemical reduction of Hg species in the environment. The reduction of Hg species to Hg^0 vapor is an important pathway for the transfer of Hg from aquatic systems to the atmosphere (*18*, *19*) and can occur by photochemical (*20*–*22*), biological (*23*, *24*), or abiotic organically mediated (*25*) mechanisms. Understanding the controls and determining the relative importance of the different reduction mechanisms is important to quantifying how much Hg is retained within an ecosystem that can be methylated and/or bioaccumulated.

Photochemical reaction experiments and MIF. We studied photochemical reduction of aqueous Hg^{+2} and MeHg by natural sunlight in a quartz reaction vessel with dissolved organic carbon (DOC). Photoreduction resulted in both MDF and MIF of Hg isotopes. In all the experiments, isotopic fractionation followed Rayleigh-type fractionation in such a way that lighter isotopes were preferentially reduced and removed from the vessel. Although the rate of the MeHg photoreduction was slower (a 20% loss after 300 min) than the rate of Hg^{+2} photoreduction (>90% loss after 300 min), the MeHg experiments resulted in larger isotopic fractionation ($^{202/198}\alpha_{product/reactant}$ = 0.9987 and 0.9983) than the Hg^{+2} experiments (α = 0.9994). No detectable MeHg was reduced during the dark abiotic control experiment, but 20% of the Hg^{+2} was reduced after 300 min in the Hg^{+2} dark control experiments, and the resulting isotopic fractionation was larger than in Hg^{+2} photoreduction (α = 0.9980 and 0.9987). This dark abiotic Hg^{+2} reduction probably resulted from organically mediated reactions (*25*). The reduction experiments were performed at Hg concentrations above environmental levels (60 to 100 ng/g) and with continuous sparging and removal of the produced Hg^0 from the reaction vessel, which hindered Hg^0 photo-oxidation. Therefore, reduction

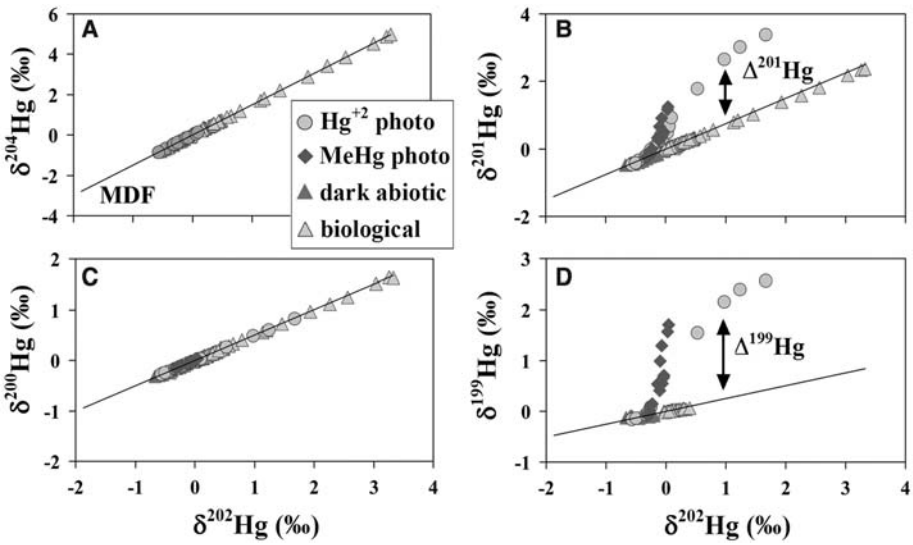

Fig. 1. Hg isotopic compositions, with δ^{202}Hg plotted against (**A**) δ^{204}Hg, (**B**) δ^{201}Hg, (**C**) δ^{200}Hg, and (**D**) δ^{199}Hg. Shown are of the Hg^{+2} photoreduction experiments, the MeHg photoreduction experiments, and dark controls from this study along with biological reduction experiments (*12*). The solid line plotted in each is the theoretically predicted MDF based on the δ^{202}Hg value (*40*, *41*). Isotopic compositions and MDF are reported in delta notation relative to a National Institute of Standards and Technology Hg standard (SRM 3133) with ^{198}Hg in the denominator: $\delta^{xxx}Hg = 1000 \times [(^{xxx/198}R_{sample}/^{xxx/198}R_{SRM\ 3133}) - 1]$, where xxx is the mass of each mercury isotope between 199 and 204 amu. For natural samples, the reproducibility of replicate analyses is typically better than ±0.15‰ (2σ, SE) for δ^{202}Hg.

Department of Geological Sciences, University of Michigan, 1100 North University Avenue, Ann Arbor, MI 48109, USA.

Downloaded from www.sciencemag.org on January 16, 2008

rates measured in our experiments are higher than rates observed in nature, and the resulting fractionation factors may not be directly applicable to natural systems. Details of the methods, nomenclature, and fractionation factors modeled for all of the reduction experiments are summarized in the supporting online material (SOM) (*26*).

The most striking observation of our experiments is that only photochemical reduction resulted in dramatic MIF [up to 2.5 per mil (‰)], and it did so only for the odd isotopes of Hg (Fig. 1). In contrast, the dark abiotic reduction experiments (this study), and the biological reduction experiments from Kritee *et al*. (*12*) followed only MDF for both the even and odd isotopes. As the photoreduction of Hg progressed, odd isotopes were preferentially retained in the reactor, with the slower MeHg photoreduction experiments displaying more MIF than the Hg^{+2} photoreduction at the same extent of reaction (Fig. 2). Furthermore, although the overall rate of reduction of MeHg in each photoreduction experiment did not change significantly with different concentrations of DOC (1 and 10 mg of C/liter; see SOM), the degree of MIF was larger for the higher-DOC experiment.

The relation between the MIF for the two odd isotopes can be used to distinguish the different photoreduction pathways and could allow for the identification of specific chemical pathways in nature. Plotting Δ^{199}Hg versus Δ^{201}Hg reveals a significant difference in the relation between the two odd isotopes for the photoreduction of Hg^{+2} versus MeHg (Fig. 3). For the Hg^{+2} photoreduction, Δ^{199}Hg and Δ^{201}Hg have similar values at the same extent of reaction. However, Δ^{199}Hg is larger than Δ^{201}Hg for the MeHg photoreduction experiments. Despite the fact that the two MeHg photoreduction experiments (1 and 10 mg of C/liter) display different degrees of MIF at the same extent of reaction (Fig. 2), the relation between Δ^{199}Hg and Δ^{201}Hg is the same for both experiments (Fig. 3). This result suggests that the reaction step that resulted in MIF for the MeHg experiments is dependent on the amount of DOC, but it is probably the same mechanism causing MIF in both MeHg experiments.

The observation of large MIF in the photochemical reduction experiments raises the question of the mechanism of isotope fractionation. MDF arises from differences in zero-point vibrational energies and thus differences in bond strengths of isotopes due to their differing masses, and can be expressed in both kinetic and equilibrium processes (*27*, *28*). Isotopic fractionation that does not follow MDF is both predicted and observed (*15*–*17*, *29*–*33*). Two of the plausible mechanisms relevant to Hg MIF are the nuclear field shift effect (*29*, *33*) and the magnetic isotope effect (*30*–*32*).

Both the nuclear field shift effect and the magnetic isotope effect predict differences in isotope fractionation between even and odd isotopes that are mass-independent. Deviation from mass-dependent scaling between isotopes occurs in the nuclear field shift effect because this effect is dependent on the nuclear volume and nuclear charge radius, which do not scale linearly with the number of neutrons. Even/odd staggering of the isotopes results because the odd isotopes have ground-state energies closer to those of the adjacent lower-mass even isotope. Nuclear field effects become more important with the increasing mass of an element and should be significant for heavier elements such as U, Hg, and Tl (*29*, *33*). In a recent modeling study (*33*), it was predicted that equilibrium isotope fractionation of Hg due to the nuclear field shift effect should be larger than mass-dependent effects, and the MIF attributable to the nuclear field shift effect should be largest for ^{199}Hg and ^{204}Hg and to a lesser extent for ^{201}Hg and ^{196}Hg.

The magnetic isotope effect is predicted to result in a more pronounced difference in the behavior of odd versus even isotopes. Only the odd isotopes have nonzero nuclear spin, nuclear magnetic moments, and hyperfine splitting. This makes the reaction rates of radical intermediates that undergo spin conversion significantly different for radical pairs that involve magnetic nuclei versus nonmagnetic nuclei (*30*–*32*). Thus, the magnetic and nonmagnetic isotopes can be preferentially accumulated in different reaction products in chemical processes with radical intermediates

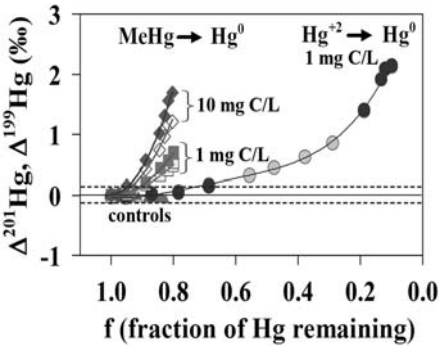

Fig. 2. MIF of reactor samples from the photoreduction experiments plotted as a function of the fraction of Hg remaining in the reactor. Three experiments along with dark abiotic controls are plotted: (●) photoreduction of Hg^{+2} with 1 mg of C/liter of DOC, (■) photoreduction of MeHg with 1 mg of C/liter of DOC, (◆) photoreduction of MeHg with 10 mg of C/liter of DOC, and (▲) dark abiotic controls. Δ^{199}Hg is plotted with the solid symbols and Δ^{201}Hg with lighter shaded symbols. MIF is reported using capital delta notation and is the deviation in the measured isotope ratios from the theoretical value based on mass-dependent kinetic isotope fractionation. δ^{202}Hg is used to establish the theoretical mass-dependent values for δ^{199}Hg and δ^{201}Hg according to the kinetic mass-dependent fractionation law (*40*, *41*), and the theoretical MDF is subtracted from the measured isotopic composition using the following formulas: $\Delta^{199}\text{Hg} = 1000 \times [(\ln((\delta^{199}\text{Hg}/1000) + 1)) - 0.2520 \times (\ln((\delta^{202}\text{Hg}/1000) + 1))]$; $\Delta^{201}\text{Hg} = 1000 \times [(\ln((\delta^{201}\text{Hg}/1000) + 1)) - 0.7520 \times (\ln((\delta^{202}\text{Hg}/1000) + 1))]$. The reproducibility of replicate analyses for natural samples for Δ^{199}Hg and Δ^{201}Hg is typically better than ±0.10‰ (2σ, SE).

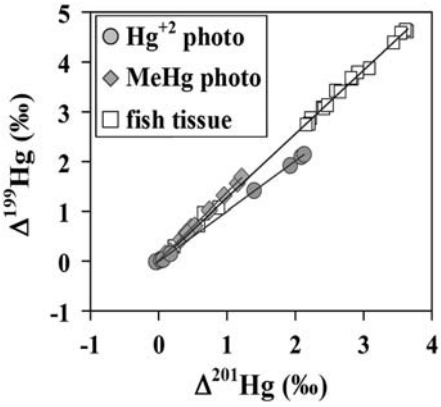

Fig. 3. Δ^{201}Hg versus Δ^{199}Hg for the photochemical reduction experiments and fish tissue samples. Dark abiotic controls all plot at the origin. The fish tissue samples plotted are from three sites in Lake Michigan. Marine dogfish (*Squalus acanthias*) reference standards [DORM-2 (muscle) and DOLT-2 (liver), see SOM] are also shown. The New England lake fish are not included because only Δ^{201}Hg was measured for these samples. The slopes are 1.36 (±0.02, 2 SE) for the MeHg photoreduction experiments, 1.00 (±0.02, 2 SE), for the Hg^{+2} photoreduction experiment, and 1.28 (±0.03, 2 SE) for the fish tissue samples.

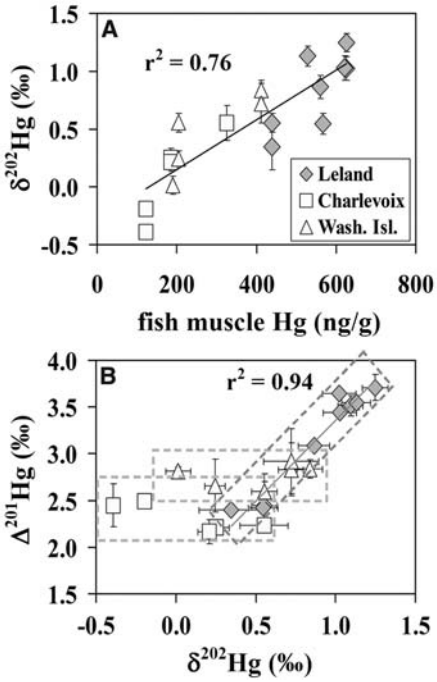

Fig. 4. (**A**) δ^{202}Hg plotted as a function of the Hg concentration (nanograms/gram) in fish muscle for burbot fish (*Lota lota*) sampled from Lake Michigan. (**B**) The MIF (Δ^{201}Hg) plotted against the MDF (δ^{202}Hg) for the same fish samples as in (A). Fish samples were collected at three sites in Lake Michigan: Leland, Charlevoix, and Washington Island. Also shown are the correlation coefficients (r^2) for all the fish samples in (A) and for the Leland site in (B).

Downloaded from www.sciencemag.org on January 16, 2008

that are branching and/or reversible. For example, in a reaction where a radical pair starts in a triplet state, the radical pairs with magnetic nuclei undergo more rapid triplet-to-singlet state conversion than the radical pairs with nonmagnetic nuclei and may preferentially recombine to regenerate the starting molecule (*31*, *32*). In contrast to the nuclear field shift effect, which can be expressed in both equilibrium and kinetic reactions, the magnetic isotope effect is purely a kinetic phenomenon.

Although we cannot unequivocally differentiate between the nuclear field shift effect and magnetic isotope effect, or a combination of these effects, it appears most likely that the magnetic isotope effect is responsible for the MIF observed in the photochemical reactions conducted in this study. The proposed mechanisms for photochemical reactions of Hg and DOC include radical intermediates such as Hg^{+} and $^{\bullet}HgCl$ (*22*, *34*), which would facilitate the magnetic isotope effect. Another observation in support of the magnetic isotope effect as the likely MIF mechanism in the photoreduction experiments is the difference in the relations between $\Delta^{199}Hg$ and $\Delta^{201}Hg$ for different reaction pathways (Fig. 3). The nuclear field shift does not provide a clear mechanism for differing fractionation patterns for different reaction pathways. The nuclear field shift effect also predicts MIF anomalies in $\Delta^{204}Hg$ (*33*), which we did not observe.

MDF and MIF of Hg isotopes in the environment. The observation of MDF and MIF in laboratory experiments raises the possibility of applying Hg isotopic variations to understand Hg in environmental systems. For instance, having an isotopic tool to help understand Hg bioaccumulation would be useful in the same way that $\delta^{15}N$ is used in food web studies (*35*). $\delta^{202}Hg$, a measure of MDF, is strongly correlated with fish muscle Hg concentrations for burbot fish (*Lota lota*) from Lake Michigan (Fig. 4A). Because the Hg concentration in fish muscle generally correlates with the size, age, and trophic level of a fish (*36*, *37*), this result suggests that $\delta^{202}Hg$ is also related to these parameters. Additionally, the Hg in fish becomes isotopically heavier with increasing Hg concentration, indicating that isotopically light Hg is excreted by fish as they age. Thus, MDF of Hg traces Hg bioaccumulation and excretion in fish.

MDF, however, is not the only isotopic signature preserved in fish. We have also found that fish display a large range in MIF (up to 4‰ in $\Delta^{201}Hg$). In a plot of $\delta^{202}Hg$ against $\Delta^{201}Hg$ (Fig. 5), representing MDF against MIF, three groups of fish samples (from Lake Michigan, New England lakes, and the ocean) occupy different regions of the plot. Different Hg sources and/or Hg transformations in aquatic ecosystems may explain contrasts in the MIF and MDF between these groups of fish. Despite these differences in the extent of MIF and MDF found in the fish muscle samples, the relation between the MIF of the two odd isotopes in all of the fish has a similar slope to that found for photoreduction of MeHg (Fig. 3). This is consistent with the finding that fish bioaccumulate mostly MeHg and that a majority (>80%) of Hg present in fish muscle is MeHg (*38*).

The similar slopes of $\Delta^{199}Hg$ versus $\Delta^{201}Hg$ for the MeHg photoreduction experiments and the fish samples suggest that the MIF observed in fish is a signature imparted to the MeHg while it was in the photic zone before it was incorporated into the food web, and that the original MIF of the MeHg remained unperturbed despite additional MDF processes occurring within the food web. This interpretation is also supported by results from two sites in Lake Michigan, for which all of the fish from a given locale have similar MIF despite large ranges in MDF (Fig. 4B). At a third site in Lake Michigan, there was a strong correlation between $\delta^{202}Hg$ and $\Delta^{201}Hg$ (Fig. 4B). Although this could indicate that there are processes during bioaccumulation in the food web that produce both MDF and MIF, it is more likely that the correlation represents a mixing line between two different sources of MeHg with two distinct signatures of MIF for this group of fish. These correlations of MDF with the size, age, and trophic level of fish, along with the MIF signatures in fish, can potentially be used to understand the sources and cycling of Hg in addition to bioaccumulation of Hg in food webs.

MIF in fish could further be used to quantify the loss of MeHg via photoreduction in aquatic ecosystems. Using the MeHg photoreduction experiment (1 mg of C/liter) and the relation between the fraction of Hg remaining in solution and $\Delta^{201}Hg$, a Rayleigh distillation model can be fit to the data and a relation derived between these parameters. This relation can then be applied to the $\Delta^{201}Hg$ preserved in fish tissues to estimate the MeHg lost via photoreduction in the ecosystem. The MIF in Lake Michigan fish suggests that ~68 ± 8% (1 SD) of the MeHg was lost via photochemical reduction before incorporation into the food web. The New England lake fish are of several species from two small lakes, and estimated losses are smaller, ~25 ± 8% and ~55 ± 8% of MeHg, for the two lakes. In general, the magnitude of the above MeHg losses via photoreduction agrees with other estimates from freshwater systems (*21*, *39*) and supports the hypothesis that this is an important pathway for the removal of MeHg from aquatic ecosystems. However, we caution that the relation between MIF and the fraction of MeHg lost via photoreduction depends on the concentration of DOC (and possibly the type of DOC) and may be site-specific, so the estimates given here will need to be confirmed with experiments using natural water from specific sites.

Implications for the global Hg cycle. Because fish, and presumably other organisms in aquatic food webs, accumulate Hg with positive MIF (enriched in the odd isotopes), a complementary reservoir must exist with negative MIF Hg (depleted in the odd isotopes). If positive MIF Hg is retained in the aqueous system after photoreduction of Hg species, then negative MIF Hg may be released to the atmosphere as Hg^0. Because Hg cycles between several active pools near Earth's surface and Hg^0 has an atmospheric residence time of about 1 year (*3*), there should be the opportunity for isotopically distinct Hg^0 to be transported away from the aquatic systems in which it was produced and be deposited elsewhere. The preservation of both MDF and MIF in environmental reservoirs of Hg will depend on the mass balance of Hg sources, but the observation of even a small degree of MIF in soils or other atmospherically derived pools would suggest that photochemical cycling of Hg species plays a substantial role in the global cycle of Hg. Thus, we expect that the MDF and MIF recorded in natural environmental samples will contribute to the understanding and quantification of important processes in the global cycle of Hg.

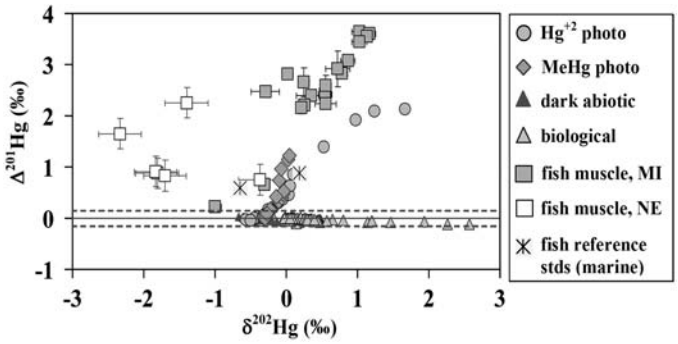

Fig. 5. MIF ($\Delta^{201}Hg$) plotted as a function of MDF ($\delta^{202}Hg$). Hg isotopic data are plotted from the photoreduction experiments, dark abiotic controls, fish muscle samples from Lake Michigan (MI) and New England (NE) lakes, and marine dogfish (*Squalus acanthias*) reference standards [DORM-2 (muscle) and DOLT-2 (liver), see SOM]. The biological reduction experiments (*12*) are plotted as well. The fish tissue samples from Lake Michigan are from burbot fish (*Lota lota*) muscle and from three locations. The fish muscle samples from the New England lakes are from two different lakes and from three species [yellow perch (*Perca flavescens*), chain pickerel (*Esox niger*), and pumpkinseed (*Lepomis gibbosus*)]. Location and sample details can be found in the SOM. Error bars are 2σ errors (2 SE) of replicate analysis except for the New England lake fish samples. These New England lake fish samples were measured earlier in the development of the method without replicates, and larger uncertainties of ±0.3‰ for $\delta^{202}Hg$ and ±0.2‰ for $\Delta^{201}Hg$ were applied to these samples.

References and Notes

1. W. F. Fitzgerald, D. R. Engstrom, R. P. Mason, E. A. Nater, *Environ. Sci. Technol.* **32**, 1 (1998).
2. C. H. Lamborg *et al.*, *Global Biogeochem. Cycles* **16**, 1104 (2002).
3. W. F. Fitzgerald, C. H. Lamborg, *Treatise Geochem.* **9**, 107 (2003).

Downloaded from www.sciencemag.org on January 16, 2008

4. T. W. Clarkson, *Environ. Health Perspect.* **100**, 31 (1993).
5. S. M. Ullrich, T. W. Tanton, S. A. Abdrashitova, *Crit. Rev. Environ. Sci. Technol.* **31**, 241 (2001).
6. D. S. Lauretta, B. Klaue, J. D. Blum, P. R. Buseck, *Geochim. Cosmochim. Acta* **65**, 2807 (2001).
7. H. Hintelmann, S. Y. Lu, *Analyst* **128**, 635 (2003).
8. H. Hintelmann, N. Ogrinc, *Am. Chem. Soc. Symp. Ser. Biogeochem. Environ. Important Trace Elements* **835**, 321 (2003).
9. T. A. Jackson, D. C. G. Muir, W. F. Vincent, *Environ. Sci. Technol.* **38**, 2813 (2004).
10. C. N. Smith, S. E. Kesler, B. Klaue, J. D. Blum, *Geology* **33**, 825 (2005).
11. D. Foucher, H. Hintelmann, *Anal. Bioanal. Chem.* **384**, 1470 (2006).
12. K. Kritee, J. D. Blum, M. W. Johnson, B. A. Bergquist, T. Barkay, *Environ. Sci. Technol.* **41**, 1889 (2007).
13. B. A. Bergquist, J. D. Blum, M. W. Johnson, A. Biswas, *Eos* **52**, Abstr. V13E-06 (2006).
14. T. A. Jackson, *Geochim. Cosmochim. Acta* **70** (suppl.), A284 (2006).
15. M. H. Thiemens, J. E. I. Heidenreich, *Science* **219**, 1073 (1983).
16. J. Farquhar, H. M. Bao, M. H. Thiemens, *Science* **289**, 756 (2000).
17. M. H. Thiemens, *Annu. Rev. Earth Planet. Sci.* **34**, 217 (2006).
18. J. P. Kim, W. F. Fitzgerald, *Science* **231**, 1131 (1986).
19. G. M. Vandal, R. P. Mason, W. F. Fitzgerald, *Water Air Soil Pollut.* **56**, 791 (1991).
20. M. Amyot, G. Mierle, D. R. S. Lean, D. J. McQueen, *Environ. Sci. Technol.* **28**, 2366 (1994).
21. P. Sellers, C. A. Kelly, J. W. M. Rudd, A. R. MacHutchon, *Nature* **380**, 694 (1996).
22. H. Zhang, *Struct. Bond Recent Dev. Mercury Sci.* **120**, 37 (2006).
23. R. P. Mason, F. M. M. Morel, H. F. Hemond, *Water Air Soil Pollut.* **80**, 775 (1995).
24. T. Barkay, J. K. Schaefer, A. J. Poulain, M. Amyot, *Geochim. Cosmochim. Acta* **69**, A702 (2005).
25. B. Allard, I. Arsenie, *Water Air Soil Pollut.* **56**, 457 (1991).
26. Additional details on experimental methods, nomenclature, and calculations are in the SOM on *Science* Online.
27. J. Bigeleisen, M. Mayer, *J. Chem. Phys.* **15**, 261 (1947).
28. H. C. Urey, *J. Chem. Soc.* **47**, 562 (1947).
29. J. Bigeleisen, *J. Am. Chem. Soc.* **118**, 3676 (1996).
30. A. L. Buchachenko, *J. Phys. Chem.* **105**, 9995 (2001).
31. V. Berdinskii, L. Yasina, A. Buchachenko, *Russ. J. Phys. Chem.* **78**, 261 (2004).
32. A. L. Buchachenko *et al.*, *Dokl. Phys. Chem.* **413**, 39 (2007).
33. E. A. Schauble, *Geochim. Cosmochim. Acta* **71**, 2170 (2007).
34. M. Ravichandran, *Chemosphere* **55**, 319 (2004).
35. M. Minagawa, E. Wada, *Geochim. Cosmochim. Acta* **48**, 1135 (1984).
36. C. A. Bache, W. H. Gutenman, D. J. Lisk, *Science* **172**, 951 (1971).
37. K. A. Kidd, R. H. Hesslein, R. J. P. Fudge, K. A. Hallard, *Water Air Soil Pollut.* **80**, 1011 (1995).
38. K. Kannan *et al.*, *Arch. Environ. Contam. Toxicol.* **34**, 109 (1998).
39. C. R. Hammerschmidt, W. F. Fitzgerald, *Environ. Sci. Technol.* **40**, 1212 (2006).
40. E. D. Young, A. Galy, H. Nagahara, *Geochim. Cosmochim. Acta* **66**, 1095 (2002).
41. J. D. Blum, B. A. Bergquist, *Anal. Bioanal. Chem.* **388**, 353 (2007).

42. We thank M. Johnson, S. Long, and A. Biswas for support and assistance in experiments and sample processing; D. Jude and C. Chen for providing fish tissue samples; and T. Barkay, K. Kritee, G. Slater, and J. Farquhar for discussions. We also thank the reviewers for their helpful comments. Funding was provided by NSF grant EAR-0433793 to J.D.B., and B.A.B. was partially supported by a Turner Postdoctoral Fellowship from the Department of Geological Sciences at the University of Michigan.

Supporting Online Material
www.sciencemag.org/cgi/content/full/1148050/DC1
Materials and Methods
Figs. S1 to S3
Tables S1 to S4
References

19 July 2007; accepted 5 September 2007
Published online 13 September 2007;
10.1126/science.1148050
Include this information when citing this paper.

Paired-End Mapping Reveals Extensive Structural Variation in the Human Genome

Jan O. Korbel,[1,2]* Alexander Eckehart Urban,[3]* Jason P. Affourtit,[4]* Brian Godwin,[4] Fabian Grubert,[5] Jan Fredrik Simons,[4] Philip M. Kim,[1] Dean Palejev,[5] Nicholas J. Carriero,[6] Lei Du,[4] Bruce E. Taillon,[4] Zhoutao Chen,[4] Andrea Tanzer,[7,8,9] A. C. Eugenia Saunders,[3] Jianxiang Chi,[10] Fengtang Yang,[10] Nigel P. Carter,[10] Matthew E. Hurles,[10] Sherman M. Weissman,[5] Timothy T. Harkins,[11] Mark B. Gerstein,[1,6,12] Michael Egholm,[4]† Michael Snyder[1,3]†

Structural variation of the genome involves kilobase- to megabase-sized deletions, duplications, insertions, inversions, and complex combinations of rearrangements. We introduce high-throughput and massive paired-end mapping (PEM), a large-scale genome-sequencing method to identify structural variants (SVs) ~3 kilobases (kb) or larger that combines the rescue and capture of paired ends of 3-kb fragments, massive 454 sequencing, and a computational approach to map DNA reads onto a reference genome. PEM was used to map SVs in an African and in a putatively European individual and identified shared and divergent SVs relative to the reference genome. Overall, we fine-mapped more than 1000 SVs and documented that the number of SVs among humans is much larger than initially hypothesized; many of the SVs potentially affect gene function. The breakpoint junction sequences of more than 200 SVs were determined with a novel pooling strategy and computational analysis. Our analysis provided insights into the mechanisms of SV formation in humans.

Structural variation of large segments (>50 kb) of the human genome was recently found to be widespread in healthy individuals (*1–4*), with ~4000 affected genomic loci currently listed in the Database of Genomic Variants (DGV) (*2*). Structural variants (SVs) may have a more significant impact on phenotypic variation than single-nucleotide polymorphisms (SNPs) (*4*, *5*). SVs have been implicated in gene expression variation (*5*), female fertility (*6*), susceptibility to HIV infection (*7*), systemic autoimmunity (*8*), and genomic disorders such as Williams-Beuren syndrome and velocardiofacial syndrome (*9*, *10*). Thus, understanding the full extent of structural variation is important for understanding phenotypic variation and genetic disease in humans.

Previous methods for detecting SVs used comparative genome hybridization—array-CGH, which involves DNA microarrays and detects copy-number variants, or CNVs (*4*) and fosmid paired-end sequencing (FPES) (*3*)—at relatively low resolution (>50 kb for array-CGH, >8 kb for FPES). Note that these methods map SVs below the resolution where breakpoints can be detected (for array-CGH) or are laborious (for FPES). Consequently, breakpoint junction sequences of a limited number of SVs and/or CNVs have been reported (*2*, *3*, *11*). Methods for comprehensively detecting SVs of <10 kb, which may encompass most variants, and for mapping breakpoints are lacking; thus, how SVs affect genes and the mechanisms by which SVs form are not known.

Development of paired-end mapping for detecting SVs. In order to identify SVs more accurately, we developed paired-end mapping (PEM), which involves the preparation and isolation of paired ends of 3-kb fragments (*12*), and their massive sequencing with 454 technology (Fig. 1) (*13*). The large number of paired-end reads was optimally mapped to the human genome computationally (*12*). Structural rearrangements were identified as significant differences between the fragments identified by the paired-end reads and the corresponding regions of the reference sequence. Five different signatures (i to v) were used to predict SVs (*12*) (Fig. 1B). (i) Deletions relative to the reference genome were identified by paired ends spanning a genomic region in the reference genome longer

[1]Molecular Biophysics and Biochemistry Department, Yale University, New Haven, CT 06520, USA. [2]European Molecular Biology Laboratory, 69117 Heidelberg, Germany. [3]Department of Molecular, Cellular, and Developmental Biology, Yale University, New Haven, CT 06520, USA. [4]454 Life Sciences, A Roche Company, Branford, CT 06405, USA. [5]Department of Genetics, Yale University School of Medicine, New Haven, CT 06520, USA. [6]Department of Computer Science, Yale University, New Haven, CT 06520, USA. [7]Department of Ecology and Evolutionary Biology, Yale University, New Haven, CT 06520, USA. [8]Department of Computer Science, University of Leipzig, 04107 Leipzig, Germany. [9]Institute for Theoretical Chemistry, University of Vienna, 1090 Vienna, Austria. [10]The Wellcome Trust Sanger Institute, Hinxton, Cambridge, CB10 1SA, UK. [11]Roche Applied Science, Indianapolis, IN 46250, USA. [12]Program in Computational Biology and Bioinformatics, Yale University, New Haven, CT 06520, USA.

*These authors contributed equally to this work.
†To whom correspondence should be addressed. E-mail: megholm@454.com (M.E.); michael.snyder@yale.edu (M.S.)

Downloaded from www.sciencemag.org on January 16, 2008

Supplemental Materials for

Bergquist, B.A., Blum, J.D. Mass-dependent and mass-independent fractionation of Hg isotopes in aquatic systems. *Submitted to Science July 2007*.

Methods

Reagents and Equipment: All acids (trace metal grade) and other reagents used in this study were purged overnight with Hg-clean Ar in order to remove any residual Hg and the deionized (DI) water used was Millipore (18 MΩ) water. Glassware and Teflon vials were cleaned with both 10% HCl and 1% BrCl followed by rinsing with DI water.

Photochemical reactor set-up (Fig. S1): Photochemical reductions of both Hg^{+2} and MeHg were performed in a quartz reaction chamber (Erlenmeyer flask) using natural sunlight (rooftop of Department of Geological Sciences, University of Michigan, Ann Arbor, MI). Experiments were performed during the day (around the maximum sunlight hour of noon) during the months of July and August 2006. Dissolved organic carbon (DOC) was used in each experiment and was Suwannee River Fulvic Acid Standard from the International Humic Substances Society (www.ihss.gatech.edu).

All experiments had an initial Hg concentration of between 60 and 100 ng/g. The Hg^0 vapor produced during the reaction was removed by continuous sparging of the reaction vessel with ambient air, which was passed through both a 0.2 μm filter and a gold trap prior to the reaction vessel in order to remove particles and Hg. Dark control experiments were performed identical to photo-reduction experiments except the reaction vessel was covered in aluminum foil, except for one dark control for Hg^{+2} that was performed in the lab in a light isolation box. The reservoir was sampled as the reactions progressed with a syringe connected to tubing. The sampling of the reservoir removed volume as the reaction progressed, but this was limited to not more than half of the initial reservoir volume. Reservoir sub samples were then preserved with 2% BrCl (Hg-clean) in glass vials with Teflon lined caps. In addition to dark controls, one Hg-free (blank) experiment was performed and no detectable Hg was observed.

The photochemical reduction rates for the Hg species measured in our experiments are higher than natural rates (*1-3*). The high rates in our experiments are

likely due to both the high initial concentrations of Hg used in the experiments and the continuous sparging and removal of Hg^0. In natural systems, Hg^0 undergoes significant photo-oxidation before removal from aqueous systems (*4, 5*).

Mercury in fish samples: Fish tissue samples were freeze-dried to remove most of the water, which was 73±4% (1SD) of the weight of the muscle samples. Mercury from fish tissues was extracted by microwave digestion (400 psi, 20 min) with a 4:1 mixture of HNO_3:HCl. Approximatley 0.5 g of freeze dried fish tissue was placed in a Teflon microwave digestion vessel and 6 ml of acid was added to each vessel. Samples were allowed to digest for at least 24 hours loosely capped. After 24 hours, 5 ml of DI water was added, the sample vessels were sealed, and the samples were microwave digested for 40 min (100 psi, 10 min; 250 psi, 10 min; 400 psi, 20 min). When cooled, samples were transferred to glass vials, preserved with 5% BrCl, and sealed with Teflon lined caps.

Hg concentration analysis: Concentrations of Hg in the photo-reduction reservoir sub-samples and fish digests were measured by atomic absorption spectroscopy following Sn(II) reduction (MA-2000, Nippon Instruments). Typical precisions for Hg concentrations are ±3% (1SD). The concentration data for the photo-reduction experiments is shown in Figure S2, and the experiment and fish concentrations are included in the tables. Two reference fish samples were analyzed for both Hg and Hg isotopes: DORM-2 and DOLT-2 (Certified Reference Materials, National Research Council of Canada, Ottawa, Ontario, Canada). Reference fish samples were digested along with each set of fish samples in addition to digestion blanks. Complete recovery of the Hg during the fish digestion processing was verified to 101±5% and blanks were below the detection limit. The detection limit was 0.02 ng/g for the instrument when run in high concentration mode for liquids (no gold trap pre-concentration). The blanks for the photochemical reactor set-up were also below the detection limit.

MC-ICP-MS analysis: Preserved reactor samples and fish digests were analyzed for their isotopic composition using a Nu Instruments multiple collector inductively coupled plasma mass spectrometer (MC-ICPMS) using continuous flow cold vapor generation with Sn(II) reduction (*6-9*). Instrumental mass bias was corrected using a thallium internal standard (NIST 997) and sample-standard bracketing (SSB) with NIST SRM 3133 (*8*). The Tl internal standard was added to the Hg vapor after cold vapor generation

using an Aridus desolvating nebulizer (CETAC). Prior to cold vapor generation, samples were partially reduced with hydroxylamine hydrochloride to remove excess BrCl and diluted to a final concentration of 5 to 30 ppb. The sample Hg and BrCl concentrations were matched to the concentrations of the bracketing standard (NIST SRM 3133) for a given analysis session to within 5% for Hg and 1% for BrCl. In addition, on-peak zero corrections were applied to all masses and the ^{204}Pb interference on ^{204}Hg was corrected by monitoring ^{206}Pb. The faraday cup configuration used for the Nu Plasma MC-ICPMS does not allow simultaneous collection of all of the Hg isotopes; therefore, we use two collection schemes. Analysis collection scheme 1 monitors masses 205, 203, 202, 201, 200, and 199. Analysis collection scheme 2 monitors masses 206, 205, 204, 203, 202, 201, 200, and 196. Most of the analyses in this study were collected using scheme 1. Isotope compositions are reported using delta notation and are reported as permil (‰) deviation from the SRM 3133 standard, which is determined by SSB during analysis using the following formula.

$$\delta^{xxx}\text{Hg (‰)} = ([(^{xxx}\text{Hg}/^{198}\text{Hg})_{\text{unknown}} \ / \ (^{xxx}\text{Hg}/^{198}\text{Hg})_{\text{SRM 3133}}] - 1) * 1000$$

where xxx is the mass of each mercury isotope between ^{199}Hg and ^{204}Hg. In the case of mass dependent fractionation (MDF), only one delta value needs to be reported and we recommend use of δ^{202}Hg. δ^{204}Hg gives a larger mass difference, but ^{204}Hg has much lower abundance than ^{202}Hg (6.9% versus 29.9%) and ^{204}Hg suffers from a potential isobaric interference with ^{204}Pb.

The recent recognition that Hg displays mass independent fractionation (MIF) in addition to MDF (*10, 11*) requires additional nomenclature (*8*). In this case we recommend consistency with similar nomenclature from the extensive literature on MIF of oxygen and sulfur (*12-14*). MIF is reported as the deviation in isotope ratios from the theoretical variation predicted by MDF. δ^{202}Hg was used to establish the theoretical values for δ^{199}Hg, δ^{200}Hg, δ^{201}Hg, and δ^{204}Hg following the kinetic mass-dependent fractionation law (*15*). MIF is reported using "capital delta" notation (Δ^{xxx}Hg; the deviation from mass dependency in units of ‰) and is the difference between the measured δ^{xxx}Hg and the theoretically predicted δ^{xxx}Hg.

$$\Delta^{199}\text{Hg} = 1000*([\ln((\delta^{199}\text{Hg}/1000)+1)] - 0.252*[\ln((\delta^{202}\text{Hg}/1000)+1)])$$

$$\Delta^{200}\text{Hg} = 1000*([\ln((\delta^{200}\text{Hg}/1000)+1)] - 0.502*[\ln((\delta^{202}\text{Hg}/1000)+1)])$$

$$\Delta^{201}Hg = 1000*([\ln((\delta^{201}Hg/1000)+1)] - 0.752*[\ln((\delta^{202}Hg/1000)+1)])$$

$$\Delta^{204}Hg = 1000*([\ln((\delta^{204}Hg/1000)+1)] - 1.492*[\ln((\delta^{202}Hg/1000)+1)])$$

which can be approximated for small ranges in delta (≤ 5‰) as:

$$\Delta^{199}Hg \approx \delta^{199}Hg - (\delta^{202}Hg * 0.252)$$

$$\Delta^{200}Hg \approx \delta^{200}Hg - (\delta^{202}Hg * 0.502)$$

$$\Delta^{201}Hg \approx \delta^{201}Hg - (\delta^{202}Hg * 0.752)$$

$$\Delta^{204}Hg \approx \delta^{201}Hg - (\delta^{202}Hg * 1.492)$$

All the data for isotopic compositions are shown in the following tables: Table S1 (Hg^{+2} photo-reduction experiments), Table S2 (MeHg photo-reduction experiments), and Table S3 (fish tissue samples).

Reporting of Analytical Uncertainty: The University of Michigan Biogeochemistry and Environmental Isotope Geochemistry Laboratory uses a secondary standard solution made from metallic Hg mined from Almadén Spain (UM-Almadén). We measured the isotopic composition of the UM-Almadén secondary standard relative to NIST 3133 several times within each analysis session in which samples are analyzed. During of the fall of 2006, we obtained a mean value of $\delta^{202}Hg$ of -0.54 ±0.08‰ (2SD, n=25) and mean $\Delta^{201}Hg$ value of –0.04 ±0.04‰ (2SD, n=25) when it was run in 1% to 5% BrCl matrices (Table S1 and S2). In addition to our in-house secondary sample, two reference fish tissue standards (DORM-2 and DOLT-2) were also analyzed for their Hg isotopic compositions and the data can be found in Table S3. The $\delta^{202}Hg$ and $\Delta^{201}Hg$ for DORM-2 were +0.18 ±0.08‰ (2SD, n=8) and +0.88 ±0.05‰ (2SD, n=8). The $\delta^{202}Hg$ and $\Delta^{201}Hg$ for DOLT-2 were -0.65 ±0.16‰ (2SD, n=8) and +0.59 ±0.10‰ (2SD, n=8).

For the uncertainty of a sample, we recommend using 2SE of the mean of replicate analyses unless it is smaller than the external reproducibility of the in-house secondary standard. When the 2SE sample replicates is smaller than the external reproducibility of the in-house secondary standard, the 2SD of the secondary standard should be reported as the sample uncertainty. For example, regardless of how well samples replicate during analysis, the $\delta^{202}Hg$ of samples in our lab run in a BrCl matrix can never have an uncertainty of less than 0.08‰ (the 2SD of the Almadén standard).

Calculations

Rayleigh fractionation factor calculations: Kinetic fractionation factors were determined from the results of our experiments (Table S4) using the form of the Rayleigh Distillation Equation (Equation 1) outlined by Mariotti et al., 1981 (*16*). The fractionation factor ($\alpha_{p/r}$) is defined for a kinetic reaction (reactant(R) $\rightarrow$ product(P)) with $\alpha_{p/r} = R_{product}/R_{reactant}$, where R = $^{xxx}Hg/^{198}Hg$ and xxx is 204, 202, 201, 200, or 199. Equation 1 was used to calculate the value of α using the Hg isotopic compositions measured in the reservoir (reactant). By plotting ln(f) versus the left hand side of Equation 1, the slope $[1+ 10^{-3}\alpha_{p/r}]$ can be used to estimate the fractionation factor (see Figure S2 for an example).

$$10^3 * \ln[(10^{-3}\delta^{xxx}Hg_t + 1)/(10^{-3}\delta^{xxx}Hg_0 + 1)] = (1+ 10^{-3}\alpha_{p/r}) * \ln(f) \quad \textbf{(1)}$$

where

$\delta^{xxx}Hg$ = the Hg isotopic composition of the reactant

i = initial, 0 minutes

t = t (minutes)

f = fraction of Hg remaining in the reactor = $[Hg]_t/[Hg]_i$

[Hg] = mercury in reactor (ng/g)

The uncertainty in $\alpha_{p/r}$ is based on the 2 standard error calculated for the best fit of the slope.

Fraction of MeHg loss via photo-reduction calculations: If the fish tissue is recording the extent to which MeHg was lost via photo-reduction in an aquatic ecosystem, the MIF preserved in fish could be used to quantify photo-reduction of MeHg in the aquatic ecosystem in which the fish grew. Using the MeHg photo-reduction experiment (1 mg C/L) relationship between the fraction of Hg remaining in solution and $\Delta^{201}Hg$, one can fit a Rayleigh distillation model to the data, derive a relationship, and apply this relationship to the $\Delta^{201}Hg$ preserved in fish tissues to estimate the MeHg lost via photo-reduction in the ecosystem. This estimation assumes that the MIF of the MeHg is preserved in the food web despite other MDF processes occurring.

Using the RDE described by Mariotti (1981) (*16*), one can linearize the $\Delta^{201}Hg$ data as a function of the fraction of Hg remaining in the reactor (f):

$$10^3 * \ln[(10^{-3}\Delta^{201}Hg_t + 1)/ (10^{-3}\Delta^{201}Hg_i + 1)] = S * \ln(f) \quad \textbf{(2)}$$

where

S = slope

f = fraction of Hg remaining in the reactor = $[Hg]_t/[Hg]_i$

i = initial, 0 minutes

t = t (minutes)

[Hg] = mercury in reactor (ng/g)

Using the data from the 1 mg C/L MeHg photo-reduction experiment, the left hand side of equation 2 can be plotted against ln(f) and one can calculate the slope (S). The estimated S and the measured $\Delta^{201}Hg$ in a fish sample can then be used to estimate an f for the MeHg in the aquatic ecosystem in which an organism grew if we assume that the $\Delta^{201}Hg_i = 0$.

$$\ln(f) = [10^3 * \ln(10^{-3}\Delta^{201}Hg_{fish} + 1)]/S \quad \textbf{(3)}$$

For the 1 mg C/L MeHg photo-reduction experiment, S is 2.43.

The above relationship (Equation 3) can be applied to the measured MIF in the fish tissues. The Lake Michigan burbot fish (*Lota lota*) were sampled at three locations (Leland, Charlevoix, and Washington Island). At two of the sites, Charlevoix and Washington Island, all of the fish from that locale have similar MIF despite large ranges in MDF. This suggests that the MIF is preserved within the food web and recording the original MIF of the MeHg prior to biological incorporation with no additional MIF processes occurring within the food web. The MIF observed in the fish from these two sites were used to estimate a MeHg loss via photo-reduction of ≈61±2% (1SD) at Charlevoix and ≈68±2% (1SD) at Washington Island. At the third site (Leland) there was a correlation between $\delta^{202}Hg$ and $\Delta^{201}Hg$. Although this could indicate that there are processes during bioaccumulation in the food web that impart both MDF and MIF, it is also likely that the correlation represents a mixing line between two different sources of Hg for this group of fish. Regardless of Hg provenance, an estimate of MeHg loss can be made of ≈71±7% (1SD) for this site. So overall, the MIF in the Lake Michigan fish

samples indicates that ≈68±8% (1SD) of the MeHg was lost via photo-chemical reduction.

The New England fish (Table S3) are from two lakes and are several species: yellow perch (*Perca flavescens*), chain pickerel (*Esox niger*), and pumpkinseed (*Lepomis gibbosus*). The fish samples indicate a loss of MeHg via photo-reduction of ≈25±8% (1SD) for Horseshoe Pond in New Hampshire and ≈55±8% (1SD) for Echo Lake in Vermont. The magnitude of the losses of MeHg agree with other estimates from freshwater systems (*17, 18*). For the marine dogfish (*Squalus acanthias*) reference standards, the estimate of MeHg loss via photo-reduction is ≈26±6% (1SD). In order to improve our estimates, additional experiments need to be done with natural water to establish relevant relationships between MIF and the fraction of MeHg lost via photo-reduction for a specific aquatic system and other potential mechanisms that might lead to MIF also need to be explored, especially in the marine system (*19*).

References

1. M. Amyot, G. Mierle, D. R. S. Lean, D. J. McQueen, *Environ. Sci. Technol.* **28**, 2366-2371 (1994).
2. M. Amyot, G. Mierle, D. Lean, D. McQueen, *Geochim. Cosmochim. Ac.* **61**, 975-987 (1997).
3. M. Costa, P. Liss, *Sci. Total. Environ.* **261**, 125-135 (2000).
4. J. Lalonde, M. Amyot, A. Kraepiel, F. Morel, *Environ. Sci. Technol.* **35**, 1367-1372 (2001).
5. E. Garcia, A. Poulain, M. Amyot, P. Ariya, *Chemosphere* **59**, 977-981 (2005).
6. B. Klaue, S. E. Kesler, J. D. Blum, paper presented at the Proceedings of the International Conference on Heavy Metals in the Environment, Ann Arbor, Michigan 2000.
7. C. N. Smith, S. E. Kesler, B. Klaue, J. D. Blum, *Geology* **33**, 825-828 (2005).
8. J. D. Blum, B. A. Bergquist, *Anal. Bioanal. Chem.* **388**, 353-359 (2007).
9. K. Kritee, J. D. Blum, M. W. Johnson, B. A. Bergquist, T. Barkay, *Environ. Sci. Technol.* **41**, 1889-1895 (2007).
10. B. A. Bergquist, J. D. Blum, M. W. Johnson, A. Biswas, *Eos Trans. AGU* **52**, Abstract V13E-06 (2006).
11. T. A. Jackson, *Geochim. Cosmochim. Ac.* **70**, A284 Suppl. (2006).
12. M. H. Thiemens, J. E. I. Heidenreich, *Science* **219**, 1073-1075 (1983).
13. J. Farquhar, H. M. Bao, M. H. Thiemens, *Science* **289**, 756-758 (2000).
14. M. H. Thiemens, *Annu. Rev. Earth Planet. Sci.* **34**, 217-262 (2006).
15. E. D. Young, A. Galy, H. Nagahara, *Geochim. Cosmochim. Ac.* **66**, 1095-1104 (2002).
16. A. Mariotti *et al.*, *Plant Soil* **62**, 413-430 (1981).
17. P. Sellers, C. A. Kelly, J. W. M. Rudd, A. R. MacHutchon, *Nature* **380**, 694-697 (1996).
18. C. R. Hammerschmidt, W. F. Fitzgerald, *Environ. Sci. Technol.* **40**, 1212-1216 (2006).
19. W. F. Fitzgerald, C. H. Lamborg, *Treatise on Geochemistry* **9**, 107-148 (2003).

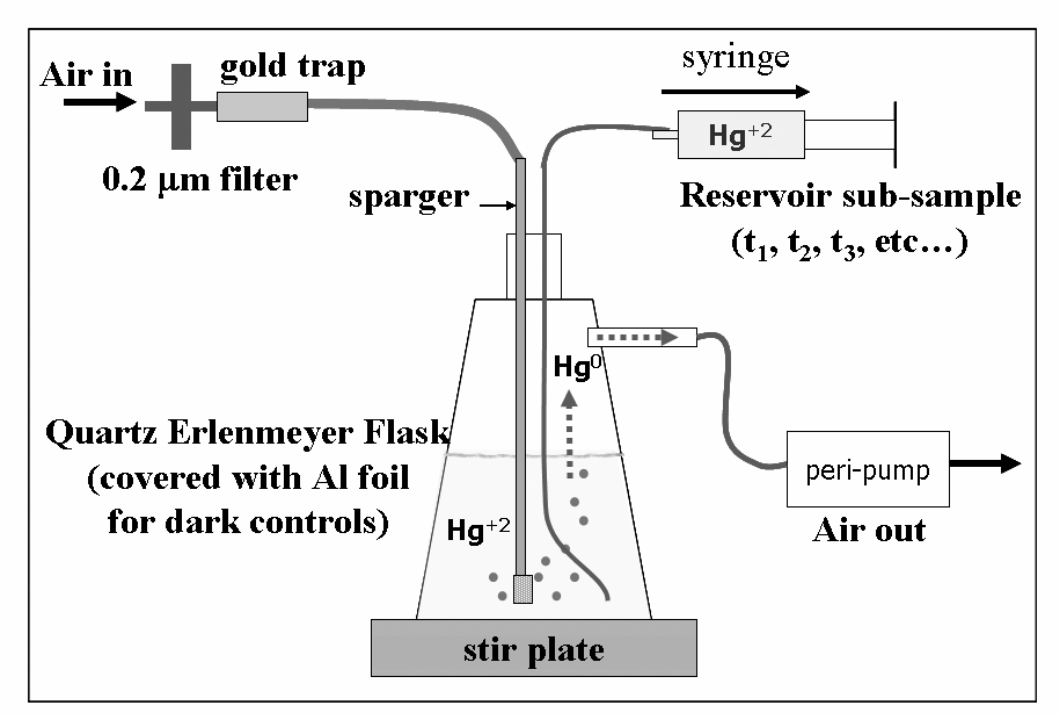

Figure S1: A schematic of the photochemical reduction apparatus.

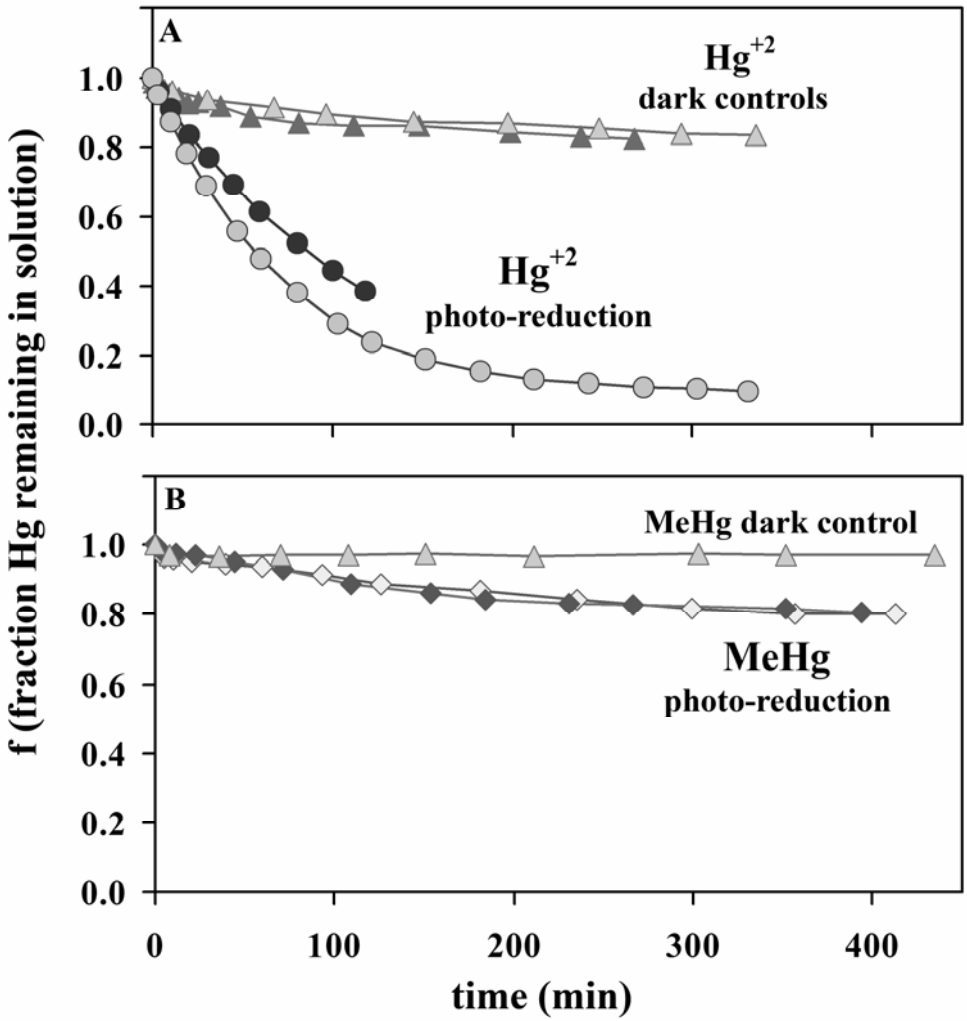

Figure S2: The fraction of Hg remaining in the reservoir for the photochemical reduction experiments plotted as a function of time. (A) The Hg^{+2} photo-reduction experiments lost ≈90% of the Hg^{+2} as Hg^0 at 300 min with a 20% loss in the Hg^{+2} dark control. (B) The MeHg photo-reduction experiments lost ≈20% of the MeHg as Hg^0 after 300 min with no measurable loss in the dark control. Initial concentrations in the experiments ranged between 60 and 100 ng/g Hg.

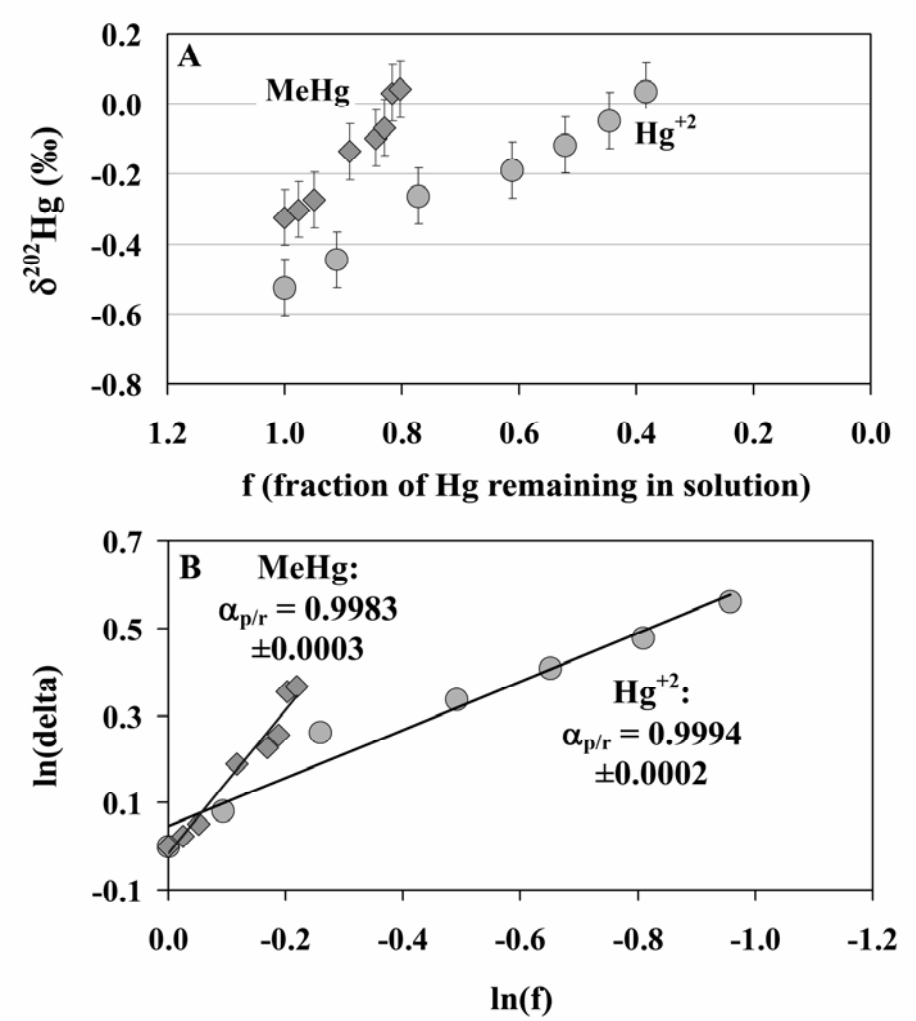

Figure S3: All of the reduction experiments followed Rayleigh type fractionation. (A) The δ^{202}Hg (‰) is plotted as a function of the fraction of Hg remaining in the reservoir (f) for one of the Hg^{+2} photo-reduction experiments and the 10 mg C/L MeHg photo-reduction experiment. Error bars are 2σ uncertainties. (B) The same data from the experiments plotted in Figure S3-A are linearized on a natural log-log plot. The left hand side of Equation 1 (ln(delta)) is plotted as a function of the natural log of the fraction of Hg remaining in the reservoir. The linearized data was used to fit a slope and calculate the fractionation factor ($\alpha_{p/r}$) for each experiment and for each isotopic ratio. Fractionation factors are summarized in Table S4. Fractionation factors may not represent natural systems because experiments were performed with higher concentrations of Hg than found in nature, and the sparging and removal of Hg^0 from the reactor likely hindered Hg^0 photo-oxidation.

Table S1: Hg isotopic compositions of the Hg^{+2} photochemical reduction experiments

expt	time (min)	Hg (ng/g)	f	δ^{202}Hg (‰)	2SD	2σ[a]	n	δ^{204}Hg (‰)	2SD	2σ[a]	n	δ^{201}Hg (‰)	2SD	2σ[a]	n	δ^{200}Hg (‰)	2SD	2σ[a]	n	δ^{199}Hg (‰)	2SD	2σ[a]	n	Δ^{204}Hg (‰)	2SD	2σ[b]	n	Δ^{201}Hg (‰)	2SD	2σ[b]	n	Δ^{200}Hg (‰)	2SD	2σ[b]	n	Δ^{199}Hg (‰)	2SD	2σ[b]	n
UM-Almadén standard				-0.54	0.08		25	-0.83	0.11		3	-0.44	0.07		25	-0.27	0.04		25	-0.14	0.06		22	0.00	0.01		3	-0.04	0.04		25	0.00	0.02		25	-0.01	0.05		22
Hg^{+2} control - UV Box																																							
R-initial	0.0	97.8	1.00	-0.48	0.10	0.08	3	-0.72	0.15	0.11	3	-0.38	0.06	0.07	3	-0.24	0.04	0.04	3					0.00	0.00	0.05	3	-0.02	0.02	0.05	3	0.00	0.02	0.05	3				
R-0	0.5	96.2	0.98	-0.54	0.08	0.08	3	-0.81	0.11	0.11	3	-0.44	0.07	0.07	3	-0.27	0.05	0.04	3					0.00	0.06	0.05	3	-0.03	0.02	0.05	3	0.00	0.05	0.05	3				
R-2	6.4	94.7	0.97	-0.54	0.15	0.09	3	-0.80	0.20	0.12	3	-0.45	0.13	0.07	3	-0.27	0.06	0.04	3					0.00	0.03	0.05	3	-0.04	0.02	0.05	3	-0.01	0.02	0.05	3				
R-4	14.6	92.4	0.94	-0.45	0.13	0.08	3	-0.66	0.22	0.13	3	-0.37	0.10	0.07	3	-0.22	0.08	0.04	3					0.01	0.03	0.05	3	-0.03	0.02	0.05	3	0.00	0.01	0.05	3				
R-6	25.5	90.7	0.93	-0.34	0.16	0.09	3	-0.51	0.25	0.14	3	-0.30	0.14	0.08	3	-0.16	0.08	0.05	3					0.00	0.00	0.05	3	-0.04	0.02	0.05	3	0.01	0.05	0.05	3				
R-8	54.7	86.7	0.89	-0.31	0.06	0.08	3	-0.48	0.08	0.11	3	-0.27	0.08	0.07	3	-0.16	0.03	0.04	3					-0.01	0.04	0.05	3	-0.04	0.04	0.05	3	0.00	0.00	0.05	3				
R-10	111.5	84.2	0.86	-0.26	0.13	0.07	3	-0.37	0.15	0.11	3	-0.23	0.10	0.07	3	-0.13	0.09	0.05	3					0.02	0.04	0.05	3	-0.04	0.01	0.05	3	0.00	0.03	0.05	3				
R-12	199.0	82.6	0.84	-0.20	0.07	0.08	3	-0.31	0.13	0.11	3	-0.20	0.08	0.07	3	-0.10	0.04	0.04	3					-0.01	0.03	0.05	3	-0.05	0.02	0.05	3	0.00	0.01	0.05	3				
R-14	268.0	80.7	0.83	-0.13	0.18	0.10	3	-0.21	0.27	0.15	3	-0.16	0.15	0.09	3	-0.07	0.07	0.04	3					-0.01	0.00	0.05	3	-0.06	0.02	0.05	3	0.00	0.02	0.05	3				
Hg^{+2} control - natrual sunlight																																							
R-initial	0.0	106.3	1.00	-0.46	0.09	0.08	3					-0.40	0.04	0.07	3	-0.24	0.03	0.04	3	-0.13	0.02	0.06	3					-0.05	0.06	0.05	3	-0.01	0.05	0.05	3	-0.02	0.04	0.05	3
R-2	10.8	102.5	0.96	-0.42	0.05	0.08	3					-0.33	0.04	0.07	3	-0.20	0.02	0.04	3	-0.12	0.03	0.06	3					-0.02	0.02	0.05	3	0.01	0.01	0.05	3	-0.01	0.02	0.05	3
R-4	67.5	97.1	0.91	-0.39	0.09	0.08	3					-0.33	0.07	0.07	3	-0.20	0.05	0.04	3	-0.10	0.04	0.06	3					-0.04	0.03	0.05	3	0.00	0.01	0.05	3	-0.01	0.02	0.05	3
R-6	145.3	92.6	0.87	-0.32	0.08	0.08	3					-0.27	0.10	0.07	3	-0.15	0.06	0.04	3	-0.10	0.03	0.06	3					-0.03	0.07	0.05	3	0.01	0.02	0.05	3	-0.02	0.02	0.05	3
R-7	197.3	92.3	0.87	-0.28	0.02	0.08	3					-0.23	0.02	0.07	3	-0.14	0.01	0.04	3	-0.10	0.01	0.06	3					-0.02	0.01	0.05	3	0.00	0.01	0.05	3	-0.03	0.01	0.05	3
R-8	248.0	90.8	0.85	-0.28	0.07	0.08	3					-0.23	0.05	0.07	3	-0.13	0.05	0.04	3	-0.09	0.05	0.06	3					-0.02	0.02	0.05	3	0.01	0.03	0.05	3	-0.02	0.04	0.05	3
R-9	294.5	89.1	0.84	-0.20	0.05	0.08	3					-0.19	0.06	0.07	3	-0.10	0.02	0.04	3	-0.08	0.04	0.06	3					-0.04	0.04	0.05	3	0.00	0.00	0.05	3	-0.03	0.03	0.05	3
R-10	335.0	88.8	0.84	-0.25	0.06	0.08	3					-0.21	0.07	0.07	3	-0.12	0.05	0.04	3	-0.08	0.02	0.06	3					-0.02	0.03	0.05	3	0.00	0.02	0.05	3	-0.02	0.01	0.05	3
Hg^{+2} - 1 mg C/L - natural sunlight																																							
R-initial	0.0	102.8	1.00	-0.53	0.07	0.08	3	-0.82	0.07	0.11	3	-0.43	0.04	0.07	3	-0.25	0.05	0.04	3					-0.04	0.04	0.05	3	-0.03	0.01	0.05	3	0.01	0.02	0.05	3				
R-1	10.2	93.7	0.91	-0.45	0.03	0.08	3	-0.68	0.03	0.11	3	-0.34	0.02	0.07	3	-0.22	0.01	0.04	3					-0.01	0.02	0.05	3	0.00	0.03	0.05	3	0.01	0.00	0.05	3				
R-3	31.0	79.4	0.77	-0.26	0.04	0.08	3	-0.40	0.03	0.11	3	-0.12	0.03	0.07	3	-0.13	0.01	0.04	3					0.00	0.03	0.05	3	0.08	0.01	0.05	3	0.00	0.02	0.05	3				
R-5	59.8	62.9	0.61	-0.19	0.08	0.08	3	-0.29	0.11	0.11	3	0.06	0.07	0.07	3	-0.09	0.05	0.04	3					-0.01	0.01	0.05	3	0.21	0.02	0.05	3	0.00	0.01	0.05	3				
R-6	80.3	53.7	0.52	-0.12	0.02	0.08	3	-0.18	0.02	0.11	3	0.21	0.06	0.07	3	-0.06	0.02	0.04	3					0.00	0.04	0.05	3	0.30	0.05	0.05	3	0.00	0.01	0.05	3				
R-7	100.0	45.8	0.45	-0.05	0.04	0.08	3	-0.09	0.06	0.11	3	0.33	0.03	0.07	3	-0.02	0.03	0.04	3					-0.02	0.01	0.05	3	0.37	0.05	0.05	3	0.00	0.02	0.05	3				
R-8	118.7	39.5	0.38	0.04	0.05	0.08	3	0.06	0.08	0.11	3	0.49	0.06	0.07	3	0.01	0.02	0.04	3					0.00	0.02	0.05	3	0.46	0.04	0.05	3	-0.01	0.01	0.05	3				
Hg^{+2} - 1 mg C/L - natural sunlight																																							
R-initial	0.0	103.0	1.00	-0.57	0.16	0.08	10	-0.84	0.08	0.11	3	-0.46	0.13	0.07	10	-0.28	0.06	0.04	10	-0.15	0.12	0.06	7	-0.04	0.04	0.05	3	-0.03	0.06	0.05	10	0.01	0.03	0.05	10	-0.01	0.13	0.05	7
R-0	3.0	98.1	0.95	-0.50	0.03	0.08	3					-0.42	0.09	0.07	3	-0.25	0.02	0.04	3	-0.14	0.08	0.06	3					-0.04	0.09	0.05	3	0.01	0.03	0.05	3	-0.01	0.07	0.05	3
R-1	10.3	89.7	0.87	-0.34	0.07	0.08	6	-0.51	0.15	0.11	3	-0.22	0.04	0.07	6	-0.17	0.06	0.04	6	-0.07	0.08	0.06	3	0.00	0.00	0.05	3	0.03	0.04	0.05	6	0.00	0.05	0.05	6	0.02	0.10	0.06	3
R-2	19.2	80.7	0.78	-0.31	0.06	0.08	6	-0.45	0.13	0.11	3	-0.17	0.10	0.07	6	-0.16	0.05	0.04	6	-0.04	0.09	0.06	3	0.01	0.05	0.05	3	0.06	0.08	0.05	6	-0.01	0.04	0.05	6	0.04	0.08	0.05	3
R-3	30.0	70.7	0.69	-0.25	0.05	0.08	5	-0.37	0.12	0.11	3	-0.02	0.08	0.07	5	-0.12	0.02	0.04	5	0.08	0.01	0.06	2	0.00	0.08	0.05	3	0.17	0.07	0.05	5	0.00	0.01	0.05	5	0.14	0.01	0.05	2
R-4	46.8	57.2	0.56	-0.11	0.04	0.08	3	-0.16	0.07	0.11	3	0.24	0.03	0.07	3	-0.05	0.04	0.04	3					0.01	0.01	0.05	3	0.32	0.01	0.05	3	0.01	0.02	0.05	3				
R-5	60.0	49.1	0.48	-0.08	0.04	0.08	3	-0.12	0.04	0.11	3	0.39	0.02	0.07	3	-0.04	0.01	0.04	3					-0.01	0.06	0.05	3	0.45	0.01	0.05	3	0.00	0.02	0.05	3				
R-6	80.3	39.0	0.38	0.06	0.03	0.08	3	0.07	0.05	0.11	3	0.67	0.05	0.07	3	0.03	0.02	0.04	3					-0.01	0.02	0.05	3	0.63	0.03	0.05	3	0.00	0.02	0.05	3				
R-7	102.8	29.8	0.29	0.09	0.06	0.08	2	0.13	0.15	0.11	2	0.93	0.09	0.07	2	0.04	0.00	0.04	2					-0.01	0.05	0.05	2	0.86	0.04	0.05	2	-0.01	0.03	0.05	2				
R-9	151.5	19.3	0.19	0.53	0.08	0.08	1					1.79	0.08	0.08	1	0.26	0.05	0.05	1	1.54	0.07	0.07	1					1.39	0.03	0.05	1	-0.01	0.02	0.05	1	1.41	0.06	0.06	1
R-11	212.0	13.7	0.13	0.98	0.18	0.10	3					2.65	0.13	0.08	3	0.49	0.07	0.04	3	2.16	0.05	0.06	3					1.92	0.03	0.05	3	0.00	0.09	0.05	3	1.91	0.05	0.02	3
R-12	242.3	12.3	0.12	1.24	0.04	0.08	3					3.02	0.06	0.08	3	0.61	0.07	0.04	3	2.39	0.06	0.06	3					2.09	0.04	0.05	3	-0.02	0.05	0.05	3	2.08	0.05	0.03	3
R-15	330.7	10.2	0.10	1.67	0.15	0.08	3					3.39	0.13	0.07	3	0.83	0.07	0.04	3	2.56	0.08	0.06	3					2.13	0.02	0.05	3	-0.01	0.03	0.05	3	2.14	0.07	0.04	3

[a]The 2σ uncertainty is the 2 standard error (2SE) of the sample replicates unless it is smaller than the 2 standard deviation (2SD) of the secondary standard (UM-Almadén). In the case where the 2SE of the sample replicates is smaller than the 2SD of the secondary standard, the 2SD of the secondary standard is applied as the uncertainty of the sample isotopic composition.

[b]The 2σ uncertainty is the 2 standard error (2SE) of the sample replicates unless it is smaller than the 2 standard deviation (2SD) of the secondary standard (UM-Almadén). In the case where the 2SE of the sample replicates is smaller than the 2SD of the secondary standard, the largest 2SD for MIF of the secondary standard is applied as the uncertainty of the sample MIF ±0.05‰).

Table S2: Hg isotopic compositions of the MeHg photochemical reduction experiments

expt	time (min)	Hg (ng/g)	f	δ^{202}Hg (‰)	2SD	2σ[a]	n	δ^{204}Hg (‰)	2SD	2σ[a]	n	δ^{201}Hg (‰)	2SD	2σ[a]	n	δ^{200}Hg (‰)	2SD	2σ[a]	n	δ^{199}Hg (‰)	2SD	2σ[a]	n	Δ^{204}Hg (‰)	2SD	2σ[b]	n	Δ^{201}Hg (‰)	2SD	2σ[b]	n	Δ^{200}Hg (‰)	2SD	2σ[b]	n	Δ^{199}Hg (‰)	2SD	2σ[b]	n
UM-Almadén standard				-0.54	0.08		25	-0.83	0.11		3	-0.44	0.07		25	-0.27	0.04		25	-0.14	0.06		22	0.00	0.01		3	-0.04	0.04		25	0.00	0.02		25	-0.01	0.05		22
MeHg control - natural sunlight																																							
R-initial	0.0	133.1	1.00	-0.62	0.02	0.08	3					-0.45	0.06	0.07	3	-0.30	0.05	0.04	3	-0.12	0.05	0.03	3					0.01	0.05	0.05	3	0.01	0.05	0.05	3	0.03	0.05	0.05	3
R-2	36.0	129.0	0.97	-0.61	0.10	0.08	3					-0.44	0.03	0.07	3	-0.29	0.03	0.04	3	-0.12	0.04	0.02	3					0.01	0.08	0.05	3	0.02	0.05	0.05	3	0.03	0.02	0.05	3
R-4	107.5	129.2	0.97	-0.60	0.24	0.17	2					-0.43	0.14	0.10	2	-0.29	0.09	0.07	2	-0.11	0.06	0.04	2					0.02	0.05	0.05	2	0.01	0.03	0.05	2	0.05	0.00	0.05	2
R-6	211.5	128.9	0.97	-0.56	0.04	0.08	2					-0.41	0.06	0.07	2	-0.27	0.04	0.04	2	-0.10	0.02	0.02	2					0.01	0.03	0.05	2	0.01	0.02	0.05	2	0.04	0.01	0.05	2
R-8	352.0	129.2	0.97	-0.67	0.13	0.08	3					-0.47	0.04	0.07	3	-0.32	0.03	0.04	3	-0.12	0.03	0.02	3					0.03	0.07	0.05	3	0.02	0.05	0.05	3	0.04	0.00	0.05	3
R-10	491.0	129.0	0.97	-0.56	0.06	0.08	3					-0.42	0.01	0.07	3	-0.27	0.03	0.04	3	-0.10	0.02	0.01	3					0.00	0.04	0.05	3	0.01	0.01	0.05	3	0.04	0.02	0.05	3
R-11	1308.0	129.1	0.97	-0.59	0.13	0.10	2					-0.44	0.09	0.07	2	-0.29	0.11	0.08	2	-0.10	0.04	0.03	2					0.01	0.01	0.05	2	0.01	0.04	0.05	2	0.05	0.01	0.05	2
R-12	1581.0	129.2	0.97	-0.57	0.13	0.09	2					-0.42	0.12	0.09	2	-0.29	0.05	0.04	2	-0.10	0.05	0.04	2					0.01	0.03	0.05	2	0.00	0.01	0.05	2	0.05	0.02	0.05	2
MeHg - 1 mg C/L - natural sunlight																																							
R-initial	0.0	66.2	1.00	-0.31	0.04	0.08	2					-0.25	0.07	0.07	2	-0.16	0.06	0.04	2	-0.07	0.03	0.02	2					-0.02	0.04	0.05	2	0.00	0.04	0.05	2	0.01	0.02	0.05	2
R-3	20.3	62.9	0.95	-0.29	0.14	0.08	3					-0.20	0.10	0.07	3	-0.13	0.10	0.06	3	-0.03	0.05	0.03	3					0.02	0.03	0.05	3	0.02	0.04	0.05	3	0.04	0.03	0.05	3
R-5	60.0	62.0	0.94	-0.27	0.03	0.08	3					-0.15	0.00	0.07	3	-0.13	0.02	0.04	3	0.01	0.07	0.04	3					0.06	0.02	0.05	3	0.01	0.00	0.05	3	0.08	0.06	0.05	3
R-7	126.0	58.8	0.89	-0.23	0.08	0.08	3					0.00	0.06	0.07	3	-0.10	0.03	0.04	3	0.14	0.06	0.04	3					0.17	0.01	0.05	3	0.02	0.01	0.05	3	0.20	0.06	0.05	3
R-9	235.5	55.7	0.84	-0.11	0.02	0.08	3					0.25	0.07	0.07	3	-0.06	0.00	0.04	3	0.41	0.05	0.03	3					0.33	0.06	0.05	3	0.00	0.01	0.05	3	0.44	0.04	0.05	3
R-10	299.0	54.1	0.82	-0.06	0.12	0.08	3					0.35	0.10	0.07	3	-0.04	0.11	0.06	3	0.55	0.06	0.04	3					0.40	0.01	0.05	3	0.00	0.05	0.05	3	0.56	0.07	0.05	3
R-11	357.0	53.0	0.80	-0.04	0.13	0.08	3					0.44	0.15	0.09	3	-0.02	0.07	0.04	3	0.67	0.10	0.06	3					0.48	0.06	0.05	3	0.00	0.00	0.05	3	0.68	0.07	0.05	3
R-12	413.0	52.9	0.80	-0.03	0.04	0.08	2					0.51	0.06	0.07	2	-0.02	0.00	0.04	2	0.70	0.01	0.00	2					0.53	0.02	0.05	2	0.00	0.02	0.05	2	0.71	0.00	0.05	2
MeHg - 10 mg C/L - natural sunlight																																							
R-initial	0.0	93.5	1.00	-0.32	0.06	0.08	3					-0.24	0.08	0.07	3	-0.16	0.03	0.04	3	-0.06	0.02	0.01	3					0.01	0.03	0.05	3	0.01	0.02	0.05	3	0.02	0.03	0.05	3
R-2	11.5	91.3	0.98	-0.30	0.10	0.08	3					-0.23	0.09	0.07	3	-0.14	0.02	0.04	3	-0.05	0.03	0.02	3					0.00	0.02	0.05	3	0.01	0.04	0.05	3	0.02	0.03	0.05	3
R-4	44.2	88.8	0.95	-0.27	0.04	0.08	3					-0.11	0.05	0.07	3	-0.12	0.04	0.04	3	0.08	0.06	0.04	3					0.10	0.06	0.05	3	0.02	0.02	0.05	3	0.15	0.06	0.05	3
R-6	109.3	83.2	0.89	-0.14	0.13	0.08	3					0.32	0.09	0.07	3	-0.07	0.09	0.05	3	0.54	0.02	0.01	3					0.42	0.01	0.05	3	0.00	0.03	0.05	3	0.57	0.03	0.05	3
R-8	184.5	79.0	0.84	-0.10	0.12	0.08	3					0.67	0.15	0.08	3	-0.03	0.07	0.04	3	0.99	0.00	0.00	3					0.74	0.08	0.05	3	0.01	0.02	0.05	3	1.02	0.03	0.05	3
R-10	266.5	77.6	0.83	-0.07	0.10	0.08	3					0.91	0.10	0.07	3	-0.03	0.06	0.04	3	1.29	0.08	0.05	3					0.96	0.05	0.05	3	0.00	0.02	0.05	3	1.31	0.07	0.05	3
R-11	352.0	76.4	0.82	0.03	0.05	0.08	3					1.17	0.06	0.07	3	0.02	0.05	0.04	3	1.57	0.07	0.04	3					1.15	0.05	0.05	3	0.01	0.03	0.05	3	1.56	0.06	0.05	3
R-12	394.0	75.1	0.80	0.04	0.14	0.08	3					1.25	0.13	0.07	3	0.03	0.03	0.04	3	1.70	0.05	0.03	3					1.22	0.02	0.05	3	0.01	0.04	0.05	3	1.69	0.05	0.05	3

[a]The 2σ uncertainty is the 2 standard error (2SE) of the sample replicates unless it is smaller than the 2 standard deviation (2SD) of the secondary standard (UM-Almadén). In the case where the 2SE of the sample replicates is smaller than the 2SD of the secondary standard, the 2SD of the secondary standard is applied as the uncertainty of the sample isotopic composition.

[b]The 2σ uncertainty is the 2 standard error (2SE) of the sample replicates unless it is smaller than the 2 standard deviation (2SD) of the secondary standard (UM-Almadén). In the case where the 2SE of the sample replicates is smaller than the 2SD of the secondary standard, the largest 2SD for MIF of the secondary standard is applied as the uncertainty of the sample MIF ±0.05‰).

Table S3: Hg isotopic compositions of the fish tissue samples

sample name	digestion date/set[a]	Hg IR run/set[b]	sampling date	location	length (mm)	weight (g)	sex	Hg in fish wet[c] tissue (ng/g)	1σ unc.	n	δ^{202}Hg (‰)	2SD	2σ[d]	δ^{204}Hg (‰)	2SD	2σ[d]	δ^{201}Hg (‰)	2SD	2σ[d]	δ^{200}Hg (‰)	2SD	2σ[d]	δ^{199}Hg (‰)	2SD	2σ[d]	Δ^{204}Hg (‰)	2SD	2σ[e]	Δ^{201}Hg (‰)	2SD	2σ[e]	Δ^{200}Hg (‰)	2SD	2σ[e]	Δ^{199}Hg (‰)	2SD	2σ[e]
Marine Standard Fish (Dogfish)																																					
average DORM-2[f]										8	0.18	0.08	0.08	0.19	0.15	0.11	1.02	0.11	0.07	0.14	0.06	0.04	1.11	0.05	0.06	-0.06	0.05	0.05	0.88	0.05	0.05	0.05	0.02	0.05	1.07	0.03	0.05
average DOLT-2[f]										8	-0.65	0.16	0.08	-0.94	0.20	0.14	0.10	0.14	0.07	-0.30	0.11	0.04	0.54	0.06	0.06	-0.02	0.04	0.05	0.59	0.11	0.05	0.03	0.05	0.05	0.71	0.06	0.05
Lake Michigan Burbot Fish Muscle																																					
16-S	30-Mar-07	9-Apr-07	8-Jun-06	Leland	804	4550	F	438	23	2	0.35	0.29	0.20				2.66	0.26	0.19	0.29	0.15	0.11	3.17	0.03	0.06				2.40	0.05	0.05	0.11	0.01	0.05	3.08	0.05	0.05
16-S	28-Mar-07	27-Apr-07	8-Jun-06	Leland	804	4550	F	438	23	2	0.55	0.13	0.08	0.70	0.11	0.36	2.86	0.11	0.30	0.38	0.09	0.27				-0.13	0.12	0.12	2.44	0.09	0.26	0.10	0.04	0.14			
18-S-a	1-Apr-07	9-Apr-07	8-Jun-06	Leland	752	3800	F	626	33	3	1.02	0.18	0.10				4.42	0.23	0.13	0.62	0.12	0.07	4.89	0.13	0.07				3.64	0.09	0.05	0.11	0.03	0.05	4.62	0.08	0.05
18-S-b	1-Apr-07	16-Apr-07	8-Jun-06	Leland	752	3800	F	626	33	6	1.17	0.22	0.09	1.54	0.11	0.32	4.50	0.44	0.18	0.70	0.11	0.05	4.96	0.18	0.10	-0.09	0.11	0.05	3.61	0.28	0.11	0.11	0.00	0.05	4.64	0.17	0.10
20-S	30-Mar-07	9-Apr-07	8-Jun-06	Leland	693	2570	M	560	28	3	0.86	0.17	0.10				3.74	0.17	0.10	0.56	0.09	0.05	4.10	0.10	0.06				3.09	0.09	0.05	0.13	0.03	0.05	3.87	0.13	0.08
22-S	1-Apr-07	9-Apr-07	8-Jun-06	Leland	606	1950	F	529	26	3	1.13	0.15	0.09				4.41	0.24	0.14	0.65	0.09	0.05	4.88	0.18	0.10				3.55	0.13	0.08	0.08	0.02	0.05	4.59	0.14	0.08
23-S	1-Apr-07	9-Apr-07	8-Jun-06	Leland	652	2490	F	567	29	3	0.54	0.16	0.09				2.83	0.18	0.10	0.39	0.12	0.07	3.20	0.07	0.06				2.42	0.08	0.05	0.11	0.05	0.05	3.05	0.04	0.05
26-S	30-Mar-07	9-Apr-07	8-Jun-06	Leland	589	1925	M	621	65	3	1.03	0.18	0.10				4.22	0.17	0.10	0.62	0.15	0.09	4.66	0.05	0.06				3.44	0.04	0.05	0.11	0.06	0.05	4.39	0.00	0.05
BR-1-S	30-Mar-07	5-Apr-07	10-May-06	Charlevoix	401	N.A.	F	123	10	2	-0.29	0.28	0.20				2.21	0.38	0.27	-0.01	0.22	0.15	3.02	0.18	0.13				2.47	0.06	0.05	0.15	0.04	0.05	3.13	0.00	0.05
BR-6-S	30-Mar-07	5-Apr-07	10-May-06	Charlevoix	594	N.A.	F	325	28	2	0.55	0.21	0.15				2.65	0.23	0.17	0.40	0.11	0.08	3.02	0.16	0.12				2.23	0.07	0.05	0.12	0.00	0.05	2.87	0.11	0.08
BR-11-S-a	1-Apr-07	5-Apr-07	9-May-06	Charlevoix	508	1370	F	185	11	2	0.25	0.11	0.08				2.40	0.12	0.08	0.29	0.13	0.09	2.82	0.08	0.06				2.21	0.03	0.05	0.16	0.08	0.05	2.75	0.05	0.05
BR-11-S-b	1-Apr-07	5-Apr-07	9-May-06	Charlevoix	508	1370	F	185	11	3	0.21	0.13	0.08				2.32	0.30	0.18	0.24	0.06	0.04	2.79	0.18	0.10				2.16	0.22	0.13	0.14	0.04	0.05	2.73	0.16	0.09
Bur100	28-Mar-07	16-Apr-07	13-Jun-06	Wash. Isl.	668	2850	F	204	15	3	0.56	0.03	0.08				3.02	0.35	0.20	0.39	0.09	0.05	3.56	0.49	0.28				2.60	0.33	0.19	0.11	0.08	0.05	3.41	0.48	0.28
Bur100	30-Mar-07	16-Apr-07	13-Jun-06	Wash. Isl.	668	2850	F	204	15	2	0.24	0.09	0.08				2.84	0.47	0.33	0.26	0.14	0.10	3.46	0.40	0.28				2.66	0.40	0.28	0.13	0.10	0.07	3.39	0.38	0.27
Bur111	28-Mar-07	27-Apr-07	14-Jun-06	Wash. Isl.	582	1510	F	412	31	5	0.78	0.17	0.08	0.91	0.20	0.54	3.43	0.13	0.06	0.50	0.16	0.07	3.88	0.17	0.10	-0.17	0.04	0.05	2.83	0.01	0.05	0.11	0.08	0.05	3.66	0.14	0.08
Bur111	30-Mar-07	16-Apr-07	14-Jun-06	Wash. Isl.	582	1510	F	412	31	2	0.72	0.24	0.17				3.47	0.31	0.22	0.50	0.13	0.09	3.97	0.09	0.07				2.92	0.49	0.35	0.13	0.01	0.05	3.78	0.15	0.11
Bur121	30-Mar-07	16-Apr-07	14-Jun-06	Wash. Isl.	485	1140	F	191	10	2	0.01	0.11	0.08				2.83	0.07	0.07	0.15	0.03	0.04	3.69	0.06	0.04				2.81	0.01	0.01	0.14	0.02	0.05	3.68	0.09	0.06
New England Fish Muscle			**fish species**	**location**																																	
ELYP120-M	2003	2003	yellow perch	Echo Lake, VT		120				1	-1.40		0.30[g]				1.20		0.30[g]	-0.61		0.30[g]							2.25		0.20[g]	0.09		0.20[g]			
ELYP30-M	2003	2003	yellow perch	Echo Lake, VT		30				1	-2.33		0.30[g]				-0.10		0.30[g]	-1.09		0.30[g]							1.65		0.20[g]	0.08		0.20[g]			
HPCP200-M	2003	2003	chain pickerel	Horseshoe Pond, NH		200				1	-0.37		0.30[g]				0.47		0.30[g]	-0.11		0.30[g]							0.75		0.20[g]	0.08		0.20[g]			
HPCP200-M	1-Apr-07	5-Apr-07	chain pickerel	Horseshoe Pond, NH		200		1230	62	6	-0.30	0.06	0.08	-0.54	0.11	0.11	0.43	0.05	0.07	-0.09	0.07	0.04	0.89	0.05	0.06	-0.05	0.04	0.05	0.66	0.01	0.05	0.07	0.04	0.05	0.96	0.02	0.05
HPCP49-M	2003	2003	chain pickerel	Horseshoe Pond, NH		49				1	-1.81		0.30[g]				-0.49		0.30[g]	-0.86		0.30[g]							0.88		0.20[g]	0.05		0.20[g]			
HPYP112-M	2003	2003	yellow perch	Horseshoe Pond, NH		112				1	-1.83		0.30[g]				-0.47		0.30[g]	-0.85		0.30[g]							0.91		0.20[g]	0.07		0.20[g]			
HPYP141-M	2003	2003	yellow perch	Horseshoe Pond, NH		141				1	-1.70		0.30[g]				-0.45		0.30[g]	-0.80		0.30[g]							0.83		0.20[g]	0.06		0.20[g]			
HPPS31-M	30-Mar-07	5-Apr-07	pumpkinseed	Horseshoe Pond, NH		31		212	11	3	-1.00	0.15	0.09				-0.53	0.15	0.08	-0.44	0.07	0.04	0.04	0.09	0.06				0.22	0.07	0.05	0.06	0.02	0.05	0.29	0.09	0.05

[a]The digestion date identifies what group the sample was digested in, and samples were run in groups of 12 for digestion.

[b]The date of the Hg isotope analysis.

[c]The Hg concentration in wet tissue. Concentrations were analyzed for freeze dried samples, but water loss was measured and used to correct the concentrations to wet tissue concentrations.

[d]The 2σ uncertainty is the 2 standard error (2SE) of the sample replicates unless it is smaller than the 2 standard deviation (2SD) of the secondary standard (UM-Almadén). In the case where the 2SE
lard, the 2SD of the secondary standard is applied as the uncertainty of the sample isotopic composition.

[e]The 2σ uncertainty is the 2 standard error (2SE) of the sample replicates unless it is smaller than the 2 standard deviation (2SD) of the secondary standard (UM-Almadén). In the case where the 2SE of the
largest 2SD for MIF of the secondary standard is applied as the uncertainty of the sample MIF (±0.05‰).

[f]The fish tissue reference standards, DORM-2 (dogfish (*Squalus acanthias*) muscle) and DOLT-2 (dogfish liver), were digested with each digestion set of fish along with a digestion blank.
Materials from the National Research Council of Canada (Ottawa, Ontario, Canada).

[g]The fish samples analyzed in 2003 were only measured once and prior to several analytical improvements. Therefore, larger uncertainties based on tests of possible analytical artifacts are applied to these samples.

Table S4: Rayleigh fractionation factors ($\alpha_{p/r}$[a]) for photochemical reduction experiments

Experiment	$^{202/198}\alpha$	2SE	$^{204/198}\alpha$	2SE	$^{201/198}\alpha$	2SE	$^{200/198}\alpha$	2SE	$^{199/198}\alpha$	2SE
Hg^{+2} dark control - light isolation box	0.9980	0.0004	0.9970	0.0006	0.9986	0.0003	0.9990	0.0002		
Hg^{+2} dark control - outdoors	0.9987	0.0003			0.9989	0.0002	0.9993	0.0001	0.9997	0.0001
Hg^{+2} - 1 mg C/L - natural sunlight	0.9994	0.0002	0.9992	0.0002	0.9991	0.0001	0.9997	0.0000		
Hg^{+2} - 1 mg C/L - natural sunlight	0.9994	0.0002	0.9992	0.0002	0.9989	0.0001	0.9997	0.0001	0.9994	0.0001
MeHg dark control - outdoors[b]										
MeHg - 1 mg C/L - natural sunlight	0.9987	0.0002			0.9965	0.0005	0.9994	0.0001	0.9964	0.0007
MeHg - 10 mg C/L - natural sunlight	0.9983	0.0003			0.9929	0.0011	0.9992	0.0001	0.9917	0.0013

[a]The fractionation factors ($\alpha_{p/r}$) were calculated for the above kinetic reactions (reactant(R)→ product(P)) using methods from Mariotti et al., 1981*(10)*.

[b]No measurable MeHg was lost in this experiment, therefore fractionation factors were not estimate